nature communications

Article

https://doi.org/10.1038/s41467-026-68837-y

# Evolution of manganese low-energy photoredox catalysis from high-energy visible light photocatalysis

Received: 17 July 2025

Accepted: 15 January 2026

Published online: 27 January 2026

Check for updates

Wei Yang[1,6], Yawen Song[1,6], Xuehan Yu[1,6], Meng Tian[1], Yu Lan[1,2,3,4] ✉, Ya-Nan Wang[3], Xiaoyu Jiang[1], Shihan Liu[5], Wenjing Zhang[1] ✉, Shi-Jun Li[1,2] ✉ & Linbin Niu[1,2] ✉

Reducing the energy input of light in photocatalytic reactions is desirable yet challenging, as modifying the light-absorbing or catalytic properties of a photocatalyst typically requires tedious preparation, resulting in a lengthy development process. Here, we overcome this limitation by achieving manganese-based low-energy photoredox catalysis through the in-situ assembly of simple Mn salts with inexpensive coordinating chemicals, thereby bypassing the need for complex pre-preparation. Assembling $Mn(acac)_2$, 2,2′-bipyridine-6,6′-diamine, and $TMSN_3$ in-situ forms a visible-light-absorbing system that, upon blue-light irradiation, generates azido radicals to drive an anti-Markovnikov hydroazidation of unactivated alkenes with $H_2O$ as the hydrogen source. Building on this assembly strategy, the combination of $Mn(acac)_3$ and $TMSN_3$ in $CH_3CN$/HFIP yields a system with a light-absorption range extended to 850 nm; this feature is further leveraged to unlock the selective aerobic hydroxyazidation of alkenes in a single step. These findings pave the way for the development of in-situ-assembled, 3 d metal-based low-energy photochemistry.

Reducing the consumption of light energy needed in photocatalytic reactions is significant. Excess inputs of light energy into organic chemical reactions not only result in a waste of energy, but also probably cause several intractable issues, such as over-functionalization of reactants and incompatibility with light-sensitive/labile functional groups[1–3]. In this context, the direct use of high-energy light ($\lambda < 500$ nm)[4]—encompassing both the high-energy visible (400–500 nm) and UV (<400 nm) regions—frequently leads to an excessive input of photon energy. Furthermore, the poor penetration depth and biocompatibility of high-energy light significantly limit its applications, particularly in scale-up synthesis and biomedical fields[5–7]. Therefore, for a given high-energy photocatalytic system, the strategy for reducing its demand for light energy is of great importance[7,8].

The natural abundance, low toxicity, and versatile catalytic reactivity of 3d metal render 3d metal-catalyzed chemical reactions extraordinarily valuable. Integrating exogenous light energy into 3d metal catalysis provides intriguing opportunities to enrich the diversity of synthetic strategies in organic synthetic chemistry[9–11]. In direct visible light-induced 3d metal catalysis, a 3d metal-based light-absorbing system—without any external photocatalyst—drives the entire catalytic cycle (Fig. 1A)[12–19]. However, current 3d metal-based photoredox catalysis relies heavily on the use of high-energy light to

[1]College of Chemistry, and Pingyuan Laboratory, Zhengzhou University, Zhengzhou, Henan, PR China. [2]Pingyuan Laboratory, State Key Laboratory of Antiviral Drugs, School of Pharmaceutical Sciences, Henan Normal University, Xinxiang, Henan, PR China. [3]School of Chemistry and Chemical Engineering, Chongqing Key Laboratory of Chemical Theory and Mechanism, Chongqing University, Chongqing, PR China. [4]State Key Laboratory of Coordination Chemistry, School of Chemistry and Chemical Engineering, Nanjing University, Nanjing, Jiangsu, PR China. [5]College of Chemistry and Molecular Sciences, Henan University, Kaifeng, Henan, PR China. [6]These authors contributed equally: Wei Yang, Yawen Song, Xuehan Yu. ✉e-mail: lanyu@cqu.edu.cn; zhangwj@zzu.edu.cn; lishijunzong@zzu.edu.cn; nlb@zzu.edu.cn

achieve the desired catalytic effect. The unique mildness and deep-tissue penetration of low-energy light ($\lambda > 595$ nm) motivated us to develop a low-energy, 3d metal-based photocatalytic system[7,20–22]. Such a system holds great promise for applications across synthetic organic chemistry, biomedicine, and polymer science[7,23].

The in-situ assembly of a 3d metal-based photocatalytic system from readily available components—such as metal salts, ligands, or substrates—is a straightforward strategy for controlling both light-absorbing and catalytic properties through modulating the ligand, counterion, or metal oxidation state (Fig. 1B)[24,25]. This paradigm avoids the preparation process of 3 d metal photocatalysts and is expected to enable a rapid shift from prevalent high-energy to low-energy photoredox catalysis platforms[25].

We observed that Mn-based photocatalysis still remains in its infancy[26–43]. To date, CO-coordinated Mn(0) complexes (e.g., $Mn_2(CO)_{10}$) have been extensively studied as robust photocatalysts to mediate atom transfer or single electron transfer processes for the production of various carbon-centered radicals[44–48]. By contrast, *N*-centered radicals generated by a Mn(II or III)-based photocatalytic system remain to be developed. Given the privileged status of *N*-centered radicals in synthetic organic chemistry[49–52] and the limitations of existing systems, we questioned whether an effective Mn(II or III)-based photocatalytic platform that allows for the controllable absorption of light energy could be devised using easy-to-access starting materials to yield versatile *N*-centered radicals[53].

Here, we demonstrate that assembling Mn-based photocatalytic systems in situ is an effective strategy to rapidly unlock a low-energy photoredox catalytic system from high-energy visible light-induced Mn catalysis (Fig. 1C). The formation of valuable azido radicals can be achieved not by leveraging high-energy visible light (blue light, $\lambda_{center} = 440$ nm), but by using low-energy, near-infrared light ($\lambda_{center} = 850$ nm). The blue light-induced Mn photocatalytic system enables the anti-Markovnikov hydroazidation of unactivated alkenes with $H_2O$ as the hydrogen source, while the Mn-based low-energy photocatalytic platform allows for the aerobic hydroxyazidation of alkenes in a single step. This showcases the unique catalytic ability of in-situ-assembled, Mn-based photocatalysis.

## Results and discussion

### Evolution of a Mn-based low-energy photocatalytic system via in-situ assembly

Our study began with UV–Vis experiments to probe the in-situ assembly of the Mn-based light-absorbing system for generating desired azido radicals (Supplementary Figs. 13–18). After continuous efforts, we found that the mixture of $Mn(acac)_2$, 2,2′-bipyridine-6,6′-diamine (**L1**) and $TMSN_3$ exhibited a distinct absorption band at approximately 475 nm, which lies within the high-energy visible light region (Fig. 2A and Supplementary Fig. 13). This peak was eliminated upon removal of any one of the three components. When the mixture was subjected to blue light irradiation ($\lambda_{center} = 440$ nm), the intensity of the absorption peak gradually decreased, indicating that the events of electron transfer and azido radical generation along with the valence change of Mn might have occurred (Fig. 2B and Supplementary Fig. 15)[25]. In addition to the prominent absorption peak at ~475 nm, the absorption tail extended into the low-energy light range. Low-energy light irradiation ($\lambda_{center} = 630$ nm) was also able to consume the Mn(II)-based light-absorbing system (Fig. 2C and Supplementary Fig. 17), whereas the consumption rate was markedly lower than that under blue light irradiation. The weaker light absorption in the region of 700–850 nm relative to 630 nm should account for the lower efficiency of the expected redox event (Fig. 2D and Supplementary Fig. 18). We therefore sought a method to enhance its absorption and corresponding photoredox activity in the 700–850 nm region. In principle, raising the valence of Mn from +2 to +3 can improve the oxidizing ability of the Mn center. This stronger oxidizing power may lower the light energy required to drive the redox event, thereby enabling the use of lower-energy light.

With this hypothesis in hand, we examined the absorption spectrum of the mixture of $Mn(acac)_3$, **L1** and $TMSN_3$. The spectrum indeed showed stronger absorption in the 700–850 nm low-energy light region (Fig. 2E and Supplementary Fig. 19). It was also worth noting that irradiation of the Mn(III)-based system with a near-infrared light source (760–918 nm, $\lambda_{center} = 850$ nm) caused a distinct decrease in absorbance (Fig. 2F and Supplementary Fig. 20). Moreover, **L1** was not essential for the absorption of the near-infrared light (Fig. 2G and Supplementary Figs. 21–24). To confirm that light irradiation triggers the formation of the valuable azido radical, we proposed an anti-Markovnikov hydroazidation of alkenes[54–63] catalyzed by the Mn-based light-absorbing systems, employing $H_2O$ as the hydrogen source (Fig. 2H and Supplementary Figs. 28, 38 and 40). As shown in Fig. 2I, the targeted hydroazidation of the unactivated alkene proceeded in good yield (**3**, 78%) under the blue light-induced, Mn(II)-based photoredox catalytic system (Supplementary Tables 1–5, Supplementary Fig. 26); the yield of **3** drastically decreased when **L1** was absent (Supplementary Figs. 32–34). Furthermore, the deuterioazidation of alkenes was observed when $H_2O$ was replaced with $D_2O$ (Supplementary Fig. 30), confirming that $H_2O$ is the source of hydrogen for the alkene hydroazidation. The low reactivity observed under irradiation at 630 nm and 850 nm might correlate with the relatively weak absorption of low-energy light by the Mn(II)-based photoredox catalytic system (Fig. 2J). The Mn(III)-based, low-energy photoredox catalytic system was also examined. Unfortunately, the yields of the target product **3** were still very low (Fig. 2J). These results led us to reevaluate the plausibility of the Mn(III)-catalyzed hydroazidation of alkenes. From a mechanistic perspective (Supplementary Figs. 40 and 41), the regeneration of $[Mn^{III}]$ from $[Mn^{II}]$ is much more difficult under external oxidant-free conditions compared with that of $[Mn^{II}]$ from $[Mn^{I}]$. This might be the real reason why the blue light-induced, Mn(II)-based photoredox catalytic system was competent to perform the hydroazidation of alkenes, but the Mn(III)-based, low-energy photoredox catalytic system was ineffective.

To unlock a Mn(III)-based, low-energy photoredox catalytic reaction, the green oxidant $O_2$ was employed to fulfill the regeneration of $[Mn^{III}]$, and the preliminary results of UV–Vis experiments showed that $O_2$ could indeed facilitate the regeneration of the Mn(III)-based light-absorbing system (Fig. 2K and Supplementary Fig. 25). This finding encouraged us to design a step-economic hydroxyazidation of alkene[64–70] catalyzed by the Mn(III)-based, low-energy photoredox catalytic platform. We envisioned harnessing a simple alkyl alcohol as cheap reductant to reduce the peroxyl alcohol intermediate in situ, enabling the one-step synthesis of the corresponding $\beta$-azido alcohol (Fig. 2L and Supplementary Figs. 39, 42, and 43). It was satisfactory that in the presence of $Mn(acac)_3$ (3.0 mol%), isobutanol (1.0 equiv.), $NH_4HCO_3$ (1.0 equiv.), and 1,1,1,3,3,3-hexafluoro-2-propanol (HFIP) as the co-solvent, a good yield 82% for **4** was obtained under the irradiation of low-energy light ($\lambda_{center} = 850$ nm) (Fig. 2M, Supplementary Tables 6–13 and Supplementary Fig. 31). This low-energy photoredox catalytic platform did not require the use of bidentate *N* ligand **L1** (Supplementary Figs. 35–37). Notably, the azido radical was captured by butylated hydroxytoluene (BHT) which also inhibited the generation of **4**, indicating that azido radical was the crucial intermediate in the low-energy photocatalytic conditions (Fig. 2N, Supplementary Fig. 29). Also, the aerobic hydroxyazidation of alkenes is unlikely to proceed via a radical chain process, as continuous irradiation with low-energy light was necessary to provide the desired product (Fig. 2O, Supplementary Fig. 27).

### Scope of substrates

Having identified the optimal conditions of the anti-Markovnikov hydroazidation and aerobic hydroxyazidation of alkenes, we next

https://doi.org/10.1038/s41467-026-68837-y

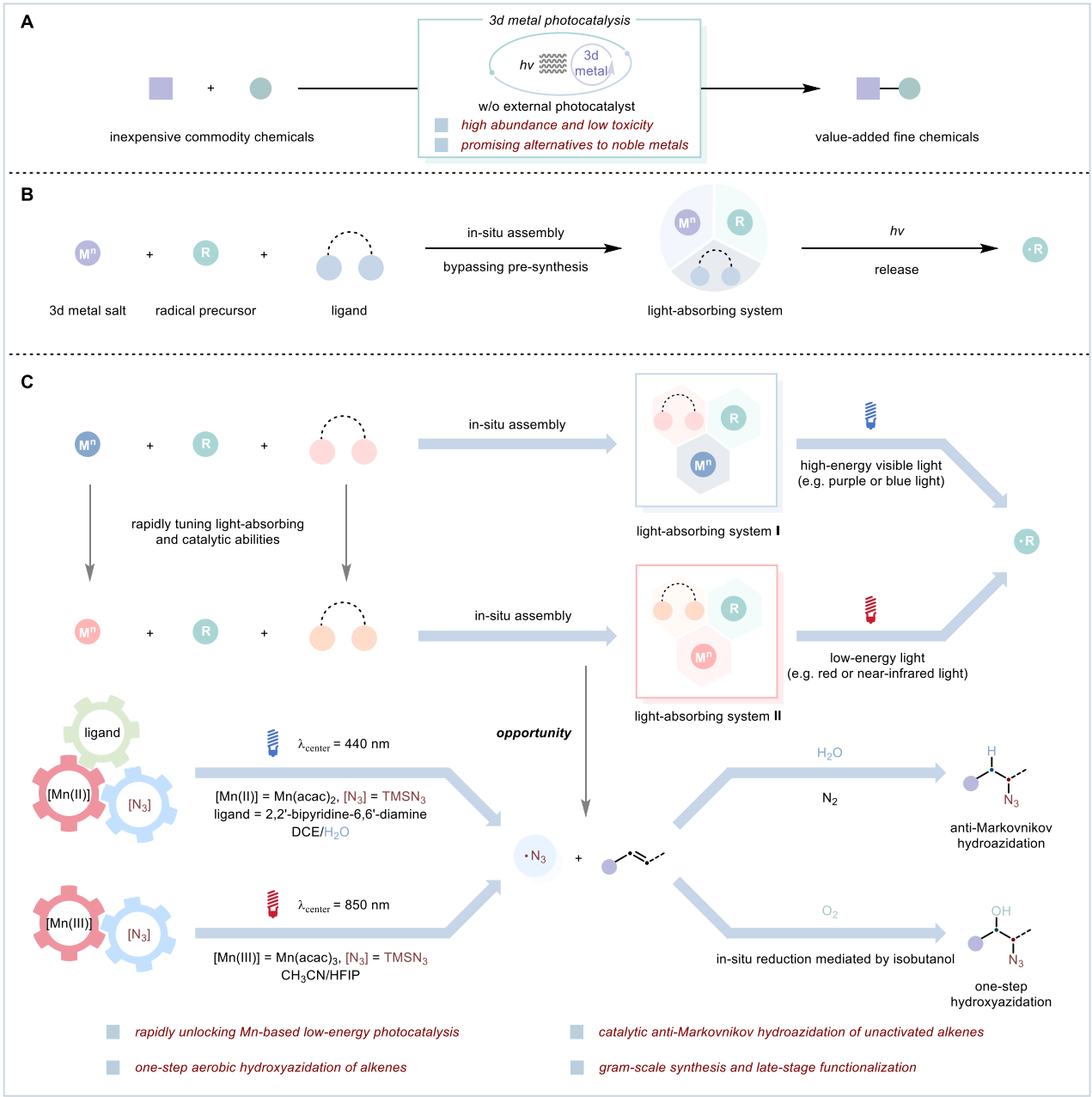


**Fig. 1 | Developing 3d metal-based photoredox catalysis for organic synthesis. A** 3d Metal-based photoredox catalysis. **B** Assembling 3d metal-based photocatalytic system in situ. **C** This work: evolution of manganese low-energy photoredox catalysis from high-energy visible light photocatalysis.

examined the substrate scope. As shown in Fig. 3, an array of alkenes was successfully converted into value-added alkyl azides in moderate to good yields (**6**–**59**). Crucially, quinoline (**16**), thioether (**40**), unprotected amine (**21** and **42**), alcohol (**26** and **31**–**59**), thiazole (**15**) and triazole (**29** and **54**) functionalities, whose coordination ability might influence the in-situ assembly of the Mn(II/III)-based light-absorbing system, did not hinder the catalytic reactivities, showcasing excellent functionality tolerance. The incorporation of $CF_3$ group (**35** and **39**) and diverse heterocycles (**12**–**17**, **29**, **30**, **54** and **55**) into alkyl azides enhanced their application potential in the field of biomedicine. Although there was a cyclopropyl in the structure of the alkene, a satisfactory yield of the hydroazidation could still be obtained (**18** and **19**). Subsequently, the late-stage functionalization of a plethora of alkenes that bear more complex molecular skeletons from various pharmaceuticals was evaluated to access new potential drug candidates. Both of the Mn-based photoredox systems generated via the strategy of in-situ assembly showed the ability to unlock complex alkyl azides with useful yields (**60**–**81**, 20%–90%) (Fig. 4, Supplementary Tables 16 and 17). In addition, the coexistence of azido and hydroxy functionalities in **74**–**81** enabled by the Mn-based low-energy photoredox catalysis further attracted the interests of biologists and pharmacologists.

## Synthetic utility

The synthetic utility and advantage of the in-situ assembly paradigm for Mn-based photocatalysis were further demonstrated. The hydroazidation and hydroxyazidation of alkenes were both synthetically scalable, and of particular note was that natural sunlight was

https://doi.org/10.1038/s41467-026-68837-y

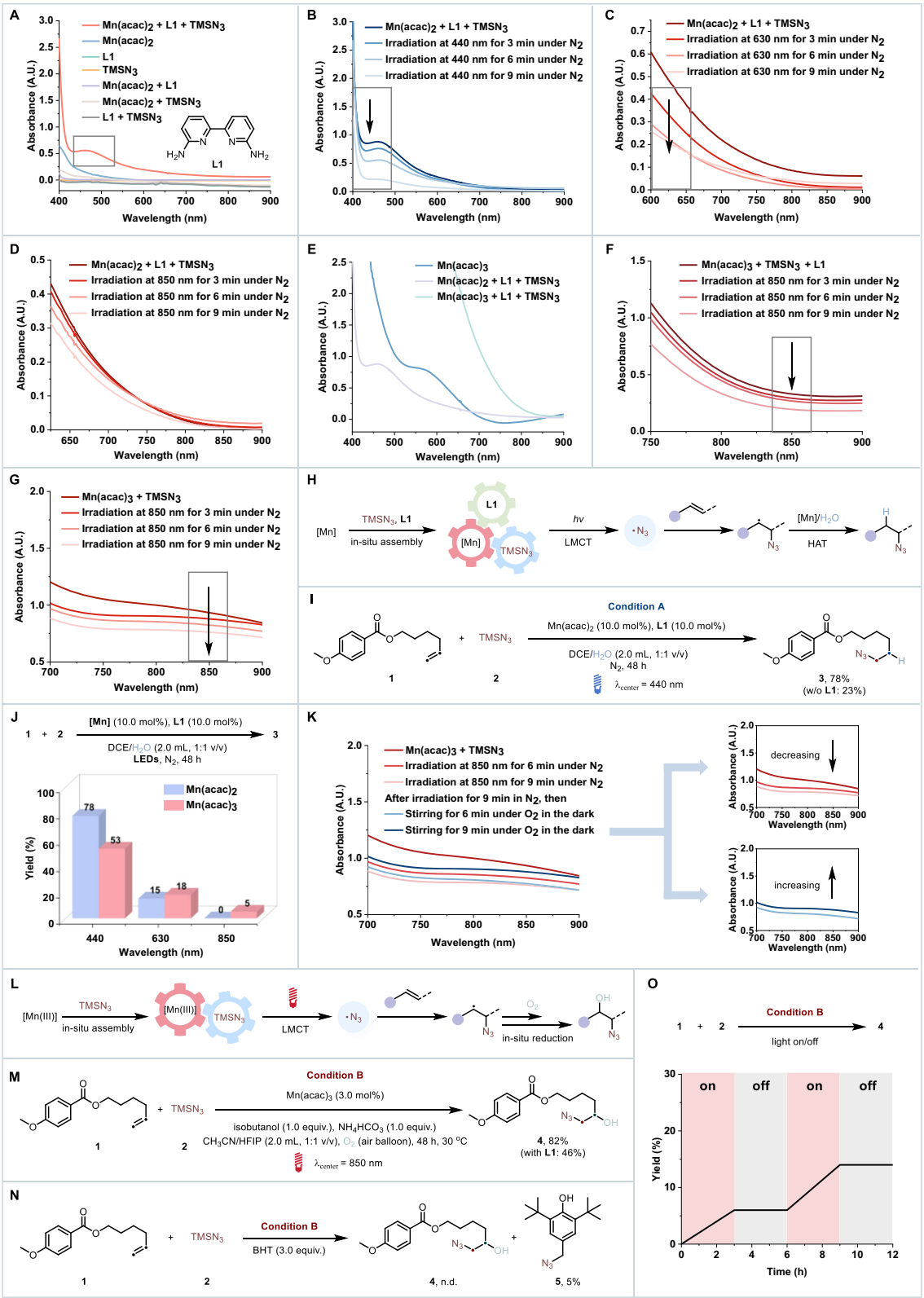


**Fig. 2 | Evolution of Mn-based low-energy photoredox catalysis. A** UV–Vis absorption spectra of the Mn(II)-based photochemical system. **B** UV–Vis monitoring of the Mn(II)-based photochemical system under 440 nm irradiation. **C** UV–Vis monitoring of the Mn(II)-based photochemical system under 630 nm irradiation. **D** UV–Vis monitoring of the Mn(II)-based photochemical system under 850 nm irradiation. **E** UV–Vis absorption spectra of the Mn(II/III)-based photochemical system. **F** UV–Vis monitoring of the Mn(III)-based photochemical system under 850 nm irradiation. **G** UV–Vis monitoring of the $Mn(acac)_3$ and $TMSN_3$ mixture upon 850 nm irradiation. **H** Design of anti-Markovnikov hydroazidation of alkenes. **I** Model reaction of the hydroazidation of alkenes. **J** Hydroazidation reactivity comparison of the Mn(II) vs. Mn(III) system under different light sources. **K** UV–Vis monitoring of the regeneration of Mn(III)-based photochemical system under $O_2$ atmosphere. **L** Design of one-step aerobic hydroxyazidation of alkenes. **M** Model reaction of one-step aerobic hydroxyazidation of alkenes. **N** Radical capture experiment with BHT in the hydroxyazidation reaction. **O** Light on/off experiment.

https://doi.org/10.1038/s41467-026-68837-y

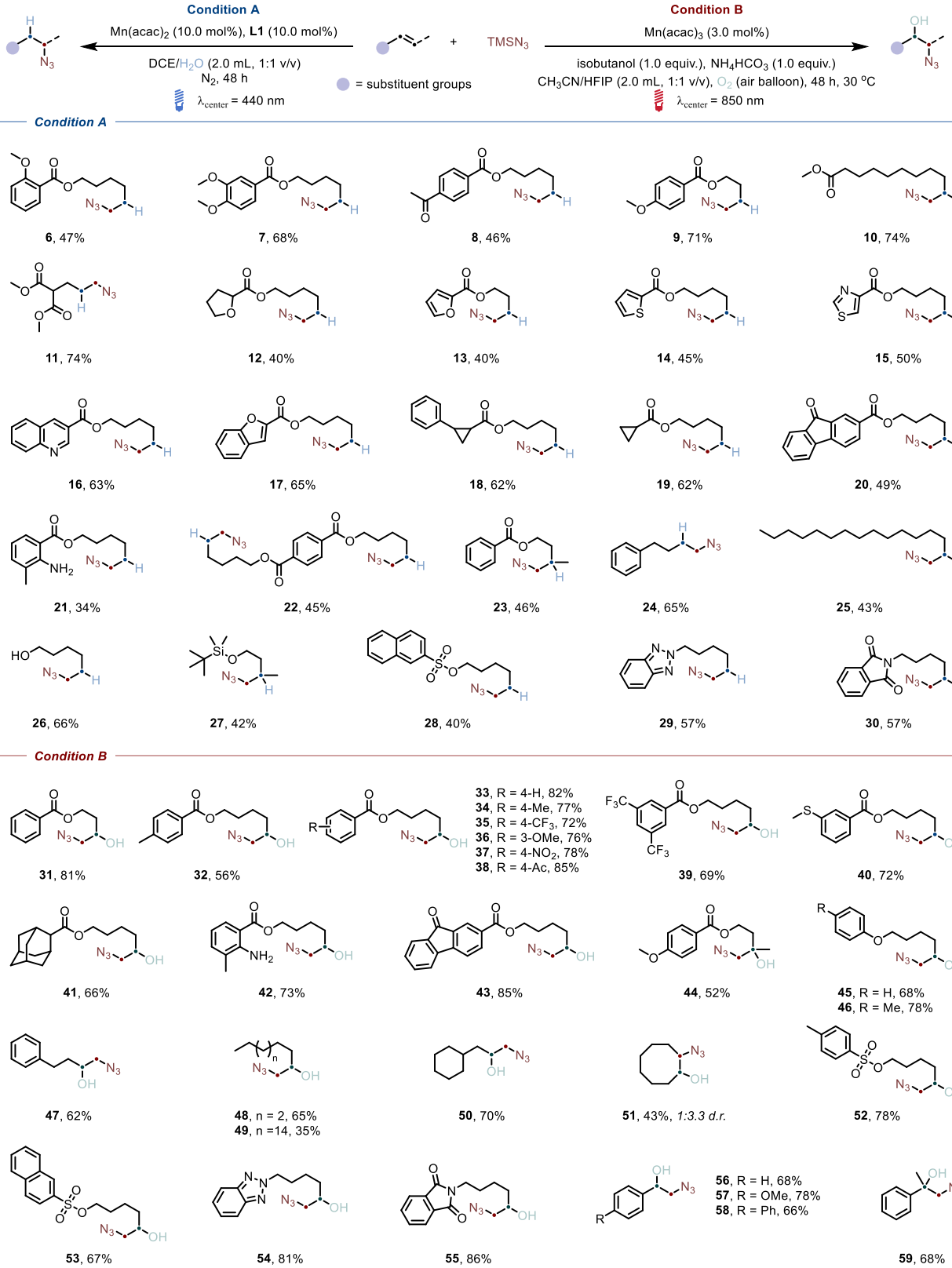


**Fig. 3 | Substrate scope.** Products were purified by silica gel chromatography to afford the isolated yields. Reaction condition A: a mixture of alkene (0.2 mmol), $TMSN_3$ (0.6 mmol), $Mn(acac)_2$ (10.0 mol%) and **L1** (10.0 mol%) in 1,2-dichloroethane (DCE)/$H_2O$ (2.0 mL, 1:1 v/v) was stirred under nitrogen atmosphere and irradiated by 440 nm light at room temperature for 48 h. Reaction condition B: a mixture of alkene (0.2 mmol), $TMSN_3$ (0.6 mmol), $Mn(acac)_3$ (3.0 mol%), isobutanol (1.0 equiv.) and $NH_4HCO_3$ (1.0 equiv.) in HFIP/$CH_3CN$ (2.0 mL, 1:1 v/v) was stirred under air atmosphere and irradiated by 850 nm light at 30 °C for 48 h. See the Supplementary Figs. 11, 12, 46 and 47 for details.

https://doi.org/10.1038/s41467-026-68837-y

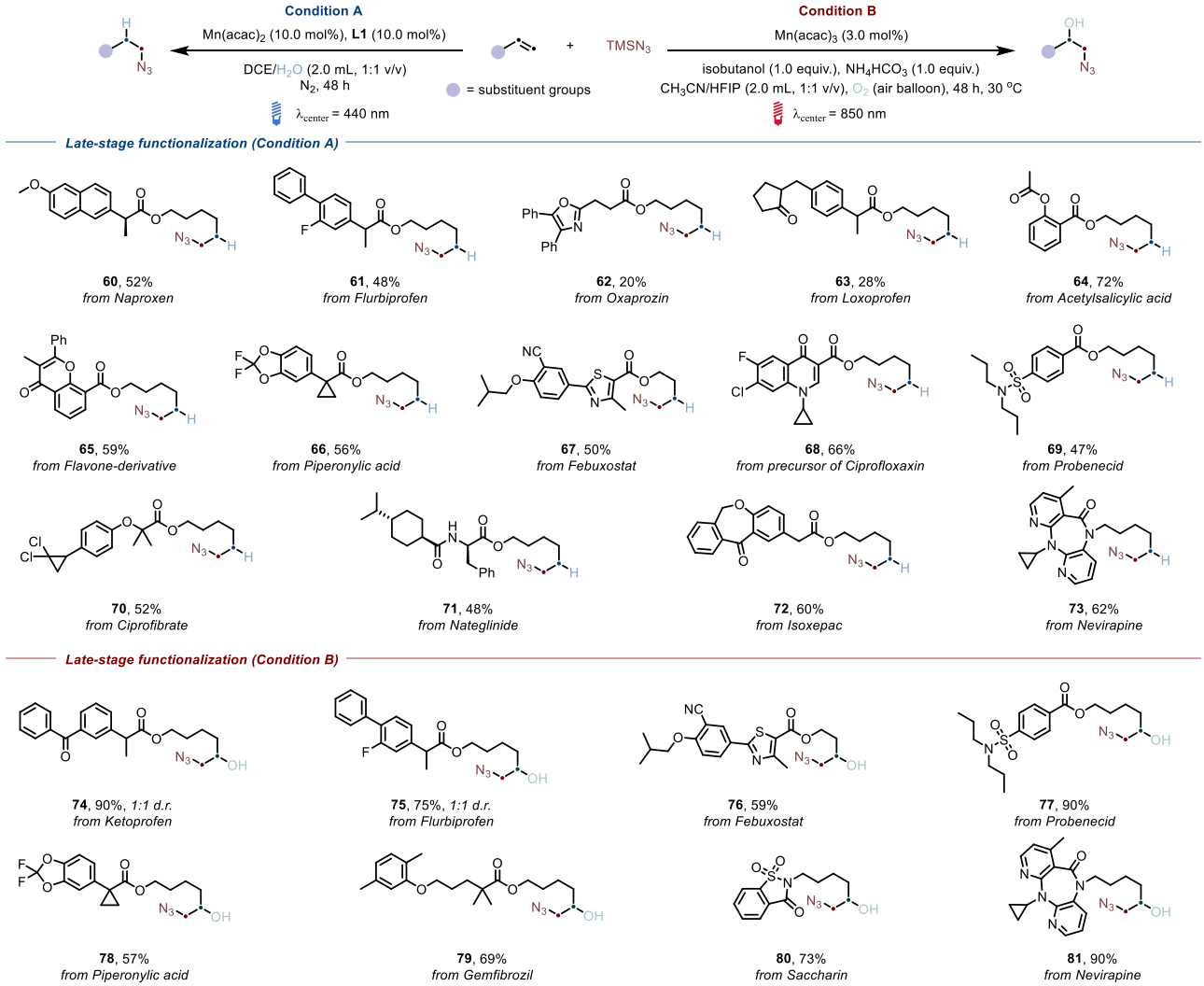


**Fig. 4 | Late-stage functionalization.** Products were purified by silica gel chromatography to afford the isolated yields. Reaction condition A: a mixture of alkene (0.2 mmol), $TMSN_3$ (0.6 mmol), $Mn(acac)_2$ (10.0 mol%) and **L1** (10.0 mol%) in DCE/$H_2O$ (2.0 mL, 1:1 v/v) was stirred under nitrogen atmosphere and irradiated by 440 nm light at room temperature for 48 h. Reaction condition B: a mixture of alkene (0.2 mmol), $TMSN_3$ (0.6 mmol), $Mn(acac)_3$ (3.0 mol%), isobutanol (1.0 equiv.) and $NH_4HCO_3$ (1.0 equiv.) in HFIP/$CH_3CN$ (2.0 mL, 1:1 v/v) was stirred under air atmosphere and irradiated by 850 nm light at 30 °C for 48 h. See the Supplementary Figs. 11, 12, 46 and 47 for details. The click reaction of alkyl azide **73** yielded the triazole derivative **S15**. The X-ray crystallographic structure of **S15** was provided in the Supplementary Information (Supplementary Table 16).

directly utilized to drive the Mn-based, low-energy photocatalytic hydroxyazidation of alkenes (Fig. 5A, Supplementary Figs. 44 and 45). During the examination of the substrate scope, we found that the alkene **82** containing an anthraquinone moiety, which itself had the ability to absorb high-energy visible light (e.g., purple or blue light), was not a competent substrate for the hydroazidation of C=C double bond (Fig. 5B-i); by contrast, only under the low-energy photocatalytic aerobic conditions (630 or 850 nm), could useful yields toward *β*-azido alcohol **84** be observed (Fig. 5B-ii). This huge disparity in reactivity between high-energy visible light photocatalysis and the low-energy photocatalysis highlighted the unique functional group tolerance of the Mn-based, low-energy photocatalytic platform. Furthermore, we found that adopting a series of current popular photocatalysts including 4CzIPN (**PC1**), $Ir[dF(CF_3)ppy]_2(dtbbpy)PF_6$ (**PC2**), $Ru(bpy)_3(PF_6)_2$ (**PC3**), and $[Acr\text{-}Mes]^+(ClO_4)^-$ (**PC4**) to catalyze the hydroazidation/hydroxyazidation of alkenes was all unsatisfactory (Fig. 5C-i). Meanwhile, the manganese-based photocatalytic system was significantly more effective than its iron-based counterpart in the hydroazidation of alkenes (Fig. 5C-ii, Supplementary Tabs. 14 and 15). Last but not least, the alkyl azide **3** and *β*-azido alcohol **4** were derivatized into a series of new organic *N*-containing compounds (**85**–**91**), further highlighting the synthetic utility of our protocol (Fig. 5D).

In conclusion, we have shown that a modular in-situ assembly strategy using easily accessible components can rapidly unlock a highly desirable Mn-based, low-energy photoredox catalytic platform, starting from a corresponding high-energy visible light photocatalysis. The Mn-based high-energy visible light photocatalysis achieves an anti-Markovnikov radical hydroazidation of unactivated alkenes with $H_2O$ as hydrogen source, and the low-energy photoredox catalytic platform enables a one-step aerobic hydroxyazidation of alkenes. The successful gram-scale synthesis and late-stage functionalization of complex molecules underscore the practical utility and broad applicability of both the Mn-based photocatalytic systems. Further efforts on the development of Mn-based low-energy photocatalytic platforms are still ongoing in our laboratory.

https://doi.org/10.1038/s41467-026-68837-y

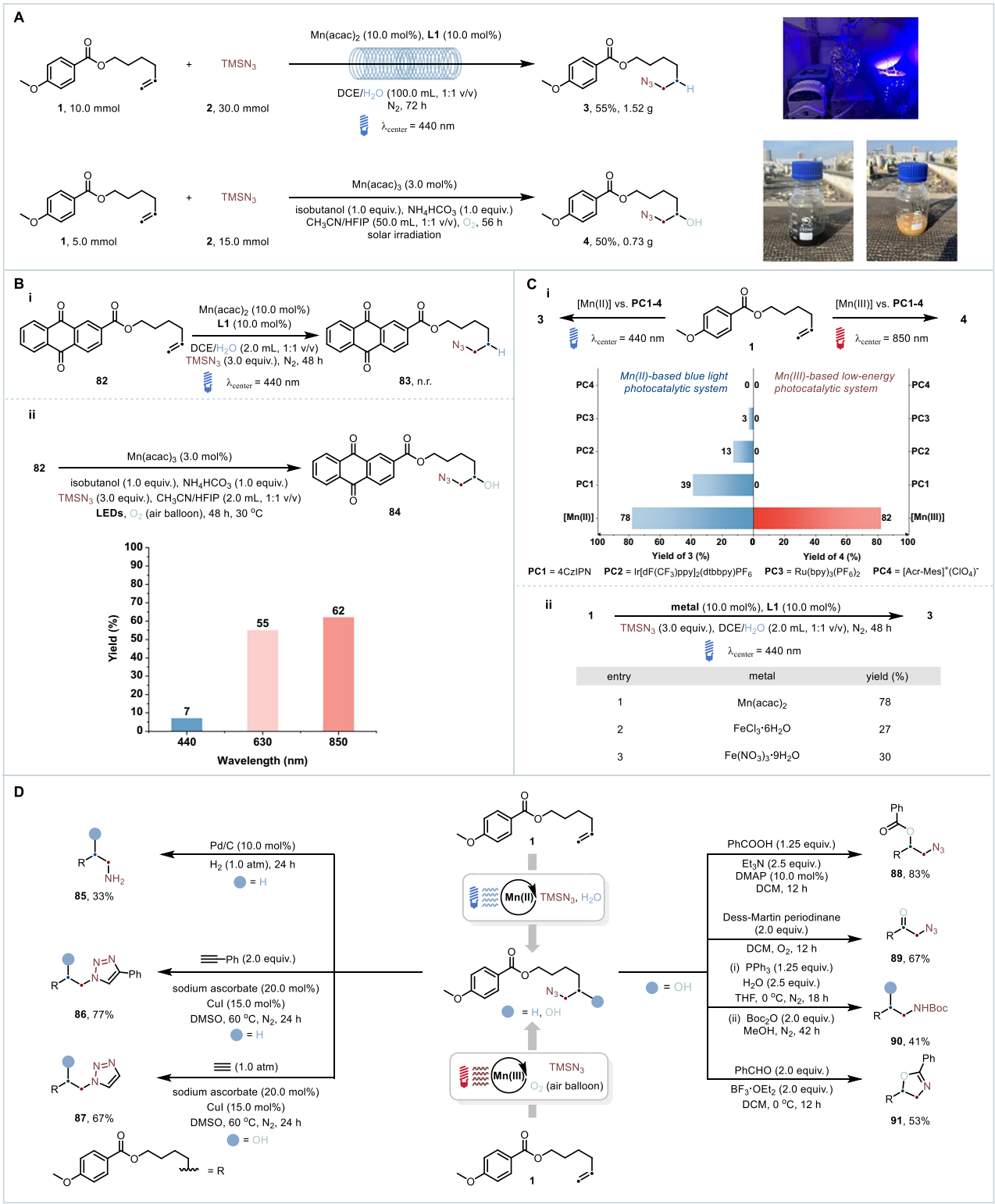


**Fig. 5 | Synthetic utility of the two Mn-based photocatalysis systems. A** Gram-scale and solar irradiation experiments. **B** Unique advantages of the Mn-based, low-energy photoredox catalytic system. The X-ray crystallographic data for *β*-azido alcohol **84** were provided in the Supplementary Information (Supplementary Tab. 17). **C** Comparisons of the two Mn-based systems and classical photocatalysts. **D** Derivatization of hydroazidation and hydroxyazidation products. (DMSO dimethyl sulfoxide, DMAP 4-dimethylaminopyridine, DCM dichloromethane, THF tetrahydrofuran).

## Methods

All reagents and catalysts were purchased from commercial sources or can be easily prepared (Supplementary Figs. 6–10), and all manipulations were carried out by standard Schlenk techniques.

### General procedure for the anti-Markovnikov hydroazidation of alkenes

To a 25.0 mL Schlenk tube that contains a stir bar were added $Mn(acac)_2$ (0.02 mmol, 10.0 mol%) and 2,2′-bipyridine-6,6′-diamine

(**L1**, 0.02 mmol, 10.0 mol%). The mixture was thoroughly degassed via vacuum-nitrogen purging and filled with nitrogen. Alkene (0.2 mmol, 1.0 equiv.), azidotrimethylsilane ($TMSN_3$, 0.6 mmol, 3.0 equiv.), $H_2O$ (1.0 mL) and anhydrous 1,2-dichloroethane (DCE, 1.0 mL) were added under nitrogen. Then the reaction was stirred and irradiated with blue light ($\lambda_{center}$ = 440 nm) at room temperature for 48 h (Supplementary Figs. 1 and 2). After the reaction was complete (monitored by TLC), the reaction mixture was extracted with ethyl acetate (EtOAc) three times. The combined organic layers were dried over $Na_2SO_4$ and removed under reduced pressure. The residue was purified by column chromatography on silica gel by eluting with petroleum ether (PE)/EtOAc to afford the products (Supplementary Figs. 11 and 46).

**General procedure for the one-step hydroxyazidation of alkenes**
To a 25.0 mL Schlenk tube that contains a stir bar were added $Mn(acac)_3$ (0.006 mmol, 3.0 mol%) and $NH_4HCO_3$ (0.2 mmol, 1.0 equiv.). The mixture was thoroughly degassed via vacuum-air purging and filled with air. Alkene (0.2 mmol, 1.0 equiv.), $TMSN_3$ (0.6 mmol, 3.0 equiv.), isobutanol (0.2 mmol, 1.0 equiv.), 1,1,1,3,3,3-hexafluoro-2-propanol (HFIP, 1.0 mL) and anhydrous $CH_3CN$ (1.0 mL) were added under air and the tube was sealed with parafilm. Then the reaction was stirred and irradiated with low-energy light ($\lambda_{center}$ = 850 nm) at 30 °C for 48 h (Supplementary Figs. 3–5). After completion of the reaction (monitored by TLC), the solvent was removed under reduced pressure. The residue was purified by column chromatography on silica gel (PE/EtOAc) to afford the products (Supplementary Figs. 12 and 47).

## Data availability

All data are available in the main text or the Supplementary Information. Data supporting the findings of this manuscript are also available from the corresponding author upon request. The X-ray crystallographic coordinates for structures reported in this study have been deposited at the Cambridge Crystallographic Data Centre (CCDC), under deposition numbers 2499393 (**84**) and 2500507 (**S15**). These data can be obtained free of charge from The Cambridge Crystallographic Data Centre via www.ccdc.cam.ac.uk/data_request/cif.

## References


1. Kurouchi, H. & Singleton, D. A. Labelling and determination of the energy in reactive intermediates in solution enabled by energy-dependent reaction selectivity. *Nat. Chem.* **10**, 237–241 (2018).
2. Wang, H., Tian, Y.-M. & König, B. Energy- and atom-efficient chemical synthesis with endergonic photocatalysis. *Nat. Rev. Chem.* **6**, 745–755 (2022).
3. Sayre, H. J. et al. Solar fuels and feedstocks: the quest for renewable black gold. *Energy Environ. Sci.* **14**, 1402–1419 (2021).
4. Tay, N. E. S. et al. Targeted activation in localized protein environments via deep red photoredox catalysis. *Nat. Chem.* **15**, 101–109 (2023).
5. Szaciłowski, K., Macyk, W., Drzewiecka-Matuszek, A., Brindell, M. & Stochel, G. Bioinorganic photochemistry: frontiers and mechanisms. *Chem. Rev.* **105**, 2647–2694 (2005).
6. Buglioni, L., Raymenants, F., Slattery, A., Zondag, S. D. A. & Noël, T. Technological innovations in photochemistry for organic synthesis: flow chemistry, high-throughput experimentation, scale-up, and photoelectrochemistry. *Chem. Rev.* **122**, 2752–2906 (2022).
7. Cabanero, D. C. & Rovis, T. Low-energy photoredox catalysis. *Nat. Rev. Chem.* **9**, 28–45 (2025).
8. Ravetz, B. D. et al. Photoredox catalysis using infrared light via triplet fusion upconversion. *Nature* **565**, 343–346 (2019).
9. Twilton, J. et al. The merger of transition metal and photocatalysis. *Nat. Rev. Chem.* **1**, 0052 (2017).
10. Chan, A. Y. et al. Metallaphotoredox: the merger of photoredox and transition metal catalysis. *Chem. Rev.* **122**, 1485–1542 (2022).
11. Skubi, K. L., Blum, T. R. & Yoon, T. P. Dual catalysis strategies in photochemical synthesis. *Chem. Rev.* **116**, 10035–10074 (2016).
12. Parasram, M. & Gevorgyan, V. Visible light-induced transition metal-catalyzed transformations: beyond conventional photosensitizers. *Chem. Soc. Rev.* **46**, 6227–6240 (2017).
13. Wenger, O. S. Photoactive complexes with earth-abundant metals. *J. Am. Chem. Soc.* **140**, 13522–13533 (2018).
14. Kancherla, R., Muralirajan, K., Sagadevan, A. & Rueping, M. Visible light-induced excited-state transition-metal catalysis. *Trends Chem.* **1**, 510–523 (2019).
15. Hockin, B. M., Li, C., Robertson, N. & Zysman-Colman, E. Photoredox catalysts based on earth-abundant metal complexes. *Catal. Sci. Technol.* **9**, 889–915 (2019).
16. Cheng, W.-M. & Shang, R. Transition metal-catalyzed organic reactions under visible light: recent developments and future perspectives. *ACS Catal.* **10**, 9170–9196 (2020).
17. Wegeberg, C. & Wenger, O. S. Luminescent first-row transition metal complexes. *JACS Au* **1**, 1860–1876 (2021).
18. Cheung, K. P. S., Sarkar, S. & Gevorgyan, V. Visible light-induced transition metal catalysis. *Chem. Rev.* **122**, 1543–1625 (2022).
19. Juliá, F. Ligand-to-metal charge transfer (LMCT) photochemistry at 3d-metal complexes: an emerging tool for sustainable organic synthesis. *ChemCatChem* **14**, e202200916 (2022).
20. Xiong, H. et al. Photo-controllable biochemistry: exploiting the photocages in phototherapeutic window. *Chem* **9**, 29–64 (2023).
21. Glaser, F. & Wenger, O. S. Sensitizer-controlled photochemical reactivity via upconversion of red light. *Chem. Sci.* **14**, 149–161 (2023).
22. Sellet, N., Cormier, M. & Goddard, J.-P. The dark side of photocatalysis: near-infrared photoredox catalysis for organic synthesis. *Org. Chem. Front.* **8**, 6783–6790 (2021).
23. Schade, A. H. & Mei, L. Applications of red light photoredox catalysis in organic synthesis. *Org. Biomol. Chem.* **21**, 2472–2485 (2023).
24. Saha, P., Jin, M. & Huang, D. C. Defluorinative C–O coupling between trifluoromethylarenes and alcohols via copper photoredox catalysis. *Angew. Chem. Int. Ed.* **64**, e202419591 (2025).
25. Yang, W. et al. Manganese low-energy photocatalysis for remodeling nitrogenation of alkenes. *Chem* **12**, 102702 (2025).
26. Jamatia, R., Mondal, A. & Srimani, D. Visible-light-induced manganese-catalyzed reactions: present approach and future prospects. *Adv. Synth. Catal.* **363**, 2969–2995 (2021).
27. Herr, P., Kerzig, C., Larsen, C. B., Häussinger, D. & Wenger, O. S. Manganese(I) complexes with metal-to-ligand charge transfer luminescence and photoreactivity. *Nat. Chem.* **13**, 956–962 (2021).
28. Huang, Z. et al. Oxidative cleavage of alkenes by $O_2$ with a non-heme manganese catalyst. *J. Am. Chem. Soc.* **143**, 10005–10013 (2021).
29. Britton, L. et al. Manganese-catalyzed C($sp^2$)–H borylation of furan and thiophene derivatives. *ACS Catal.* **11**, 6857–6864 (2021).
30. Ji, Y.-X., Li, J., Li, C.-M., Qu, S. & Zhang, B. Manganese-catalyzed N–F bond activation for hydroamination and carboamination of alkenes. *Org. Lett.* **23**, 207–212 (2021).
31. Han, J. et al. Photoinduced manganese-catalysed hydrofluorocarbofunctionalization of alkenes. *Nat. Synth.* **1**, 475–486 (2022).
32. Patra, K., Bhattacherya, A., Li, C., Bera, J. K. & Soo, H. S. Understanding the visible-light-initiated manganese-catalyzed synthesis of quinolines and naphthyridines under ambient and aerobic conditions. *ACS Catal.* **12**, 15168–15180 (2022).
33. Elsby, M. R. et al. Spin-state crossover in photo-catalyzed nitrile dihydroboration via Mn-thiolate cooperation. *Chem. Sci.* **13**, 12550–12559 (2022).
34. Joshi, A., Kumari, S. & Kundu, S. Photoredox (*NN*)Mn(I) catalysed acceptorless dehydrogenation: synthesis of amides, aldehydes and ketones. *Adv. Synth. Catal.* **364**, 4371–4383 (2022).

35. Vivien, A., Veyre, L., Mirgalet, R., Camp, C. & Thieuleux, C. $Mn_2(CO)_{10}$ and UV light: a promising combination for regioselective alkene hydrosilylation at low temperature. *Chem. Commun.* **58**, 4091–4094 (2022).
36. Mourão, H., Gomes, C. S. B., Realista, S. & Royo, B. Visible light-induced catalytic hydrosilylation of ketones mediated by manganese NHC complexes. *Appl. Organomet. Chem.* **38**, e6846 (2024).
37. Xia, S. et al. Gold-manganese bimetallic redox coupling with light. *J. Am. Chem. Soc.* **145**, 26756–26764 (2023).
38. East, N. R. et al. Oxidative two-state photoreactivity of a manganese(IV) complex using near-infrared light. *Nat. Chem.* **16**, 827–834 (2024).
39. Huang, T., Du, P., Cheng, X. & Lin, Y.-M. Manganese complexes with consecutive Mn(IV) → Mn(III) excitation for versatile photoredox catalysis. *J. Am. Chem. Soc.* **146**, 24515–24525 (2024).
40. Goncharova, I. K. et al. White-light initiated $Mn_2(CO)_{10}$/HFIP-catalyzed anti-Markovnikov hydrosilylation of alkenes. *J. Catal.* **429**, 115269 (2024).
41. Zhou, Y. et al. Photoredox-enabled manganese-catalyzed [2+2+2] cycloaddition of alkynes. *Adv. Synth. Catal.* **366**, 1545–1550 (2024).
42. Koizumi, H. et al. Development of a highly durable photocatalytic $CO_2$ reduction using a Mn-complex catalyst: application of selective photosplitting of a Mn(0)–Mn(0) bond. *J. Am. Chem. Soc.* **147**, 6236–6248 (2025).
43. Zheng, J., Chevance, S., Darcel, C. & Sortais, J.-B. Selective reduction of carboxylic acids to aldehydes through manganese catalysed hydrosilylation. *Chem. Commun.* **49**, 10010–10012 (2013).
44. Rafferty, S. M., Rutherford, J. E., Zhang, L., Wang, L. & Nagib, D. A. Cross-selective aza-pinacol coupling via atom transfer catalysis. *J. Am. Chem. Soc.* **143**, 5622–5628 (2021).
45. Laru, S., Bhattacharjee, S. & Hajra, A. Visible-light-induced Mn(0)-catalyzed direct C-3 mono-, di- and perfluoroalkylation reactions of 2*H*-indazoles. *Chem. Commun.* **58**, 13604–13607 (2022).
46. Zhong, T. et al. Manganese/cobalt bimetallic relay catalysis for divergent dehydrogenative difluoroalkylation of alkenes. *Angew. Chem. Int. Ed.* **62**, e202310762 (2023).
47. Zhou, K. et al. Ligand-assisted manganese-enabled direct C–H difluoromethylation of arenes. *Org. Chem. Front.* **11**, 4874–4881 (2024).
48. Liu, X.-G., Dong, C.-S., Li, F. & Zhang, B. Manganese-mediated direct functionalization of Hantzsch esters with alkyl iodides via an aromatization-dearomatization strategy. *Org. Lett.* **23**, 4002–4007 (2021).
49. Ge, L., Chiou, M.-F., Li, Y. & Bao, H. Radical azidation as a means of constructing $C(sp^3)$–$N_3$ bonds. *Green Synth. Catal.* **1**, 86–120 (2020).
50. Zhang, M., Zhang, J., Li, Q. & Shi, Y. Iron-mediated ligand-to-metal charge transfer enables 1,2-diazidation of alkenes. *Nat. Commun.* **13**, 7880 (2022).
51. Bian, K. J., Kao, S. C., Nemoto, D. Jr, Chen, X. W. & West, J. G. Photochemical diazidation of alkenes enabled by ligand-to-metal charge transfer and radical ligand transfer. *Nat. Commun.* **13**, 7881 (2022).
52. Shee, M. & Singh, N. D. P. Chemical versatility of azide radical: journey from a transient species to synthetic accessibility in organic transformations. *Chem. Soc. Rev.* **51**, 2255–2312 (2022).
53. Fu, N., Sauer, G. S., Saha, A., Loo, A. & Lin, S. Metal-catalyzed electrochemical diazidation of alkenes. *Science* **357**, 575–579 (2017).
54. Kapat, A., König, A., Montermini, F. & Renaud, P. A radical procedure for the anti-Markovnikov hydroazidation of alkenes. *J. Am. Chem. Soc.* **133**, 13890–13893 (2011).
55. Meyer, D. & Renaud, P. Enantioselective hydroazidation of trisubstituted non-activated alkenes. *Angew. Chem. Int. Ed.* **56**, 10858–10861 (2017).
56. Lonca, G. H. et al. Anti-Markovnikov hydrofunctionalization of alkenes: use of a benzyl group as a traceless redox-active hydrogen donor. *Angew. Chem. Int. Ed.* **56**, 11440–11444 (2017).
57. Xue, Z.-K., Fu, N.-K. & Luo, S.-Z. Asymmetric hydroazidation of α-substituted vinyl ketones catalyzed by chiral primary amine. *Chin. Chem. Lett.* **28**, 1083–1086 (2017).
58. Li, H., Shen, S.-J., Zhu, C.-L. & Xu, H. Direct intermolecular anti-Markovnikov hydroazidation of unactivated olefins. *J. Am. Chem. Soc.* **141**, 9415–9421 (2019).
59. Li, X., Chen, P. & Liu, G. Iodine(III) reagent (ABX–$N_3$)-induced intermolecular anti-Markovnikov hydroazidation of unactivated alkenes. *Sci. China Chem.* **62**, 1537–1541 (2019).
60. Wang, J.-J. & Yu, W. Anti-Markovnikov hydroazidation of alkenes by visible-light photoredox catalysis. *Chem. Eur. J.* **25**, 3510–3514 (2019).
61. Lindner, H., Amberg, W. M. & Carreira, E. M. Iron-mediated photochemical anti-Markovnikov hydroazidation of unactivated olefins. *J. Am. Chem. Soc.* **145**, 22347–22353 (2023).
62. Shi, Y., Zhang, Y., Ji, X. & Huang, H. Hydroazidation of trifluoromethyl alkenes with trimethylsilyl azide enabled by organic photoredox catalysis. *Chem. Commun.* **60**, 7741–7744 (2024).
63. Bian, K.-J. et al. Photocatalytic anti-Markovnikov hydro- and haloazidation of alkenes. *Nat. Commun.* **16**, 7906 (2025).
64. Sun, X. et al. Mn-catalyzed highly efficient aerobic oxidative hydroxyazidation of olefins: a direct approach to *β*-azido alcohols. *J. Am. Chem. Soc.* **137**, 6059–6066 (2015).
65. Yang, B. & Lu, Z. Visible-light-promoted metal-free aerobic hydroxyazidation of alkenes. *ACS Catal.* **7**, 8362–8365 (2017).
66. Xu, M.-M. et al. Dearomatization of indoles via azido radical addition and dioxygen trapping to access 2-azidoindolin-3-ols. *Org. Lett.* **21**, 6217–6220 (2019).
67. Zeng, H. et al. Three component hydroxyletherification and hydroxylazidation of (trifluoromethyl)alkenes: access to alpha-trifluoromethyl beta-heteroatom substituted tertiary alcohols. *Chem. Commun.* **56**, 6241–6244 (2020).
68. Qiao, L. et al. Visible-light-induced photocatalyst-free aerobic hydroxyazidations of indoles: a highly regioselective and stereoselective synthesis of trans-2-azidoindolin-3-ols. *J. Org. Chem.* **86**, 7955–7962 (2021).
69. Cai, Y., Jiang, H. & Zhu, C. $MnBr_2$-catalyzed aerobic oxyazidation of fluoroolefins: access to fluoroalkylated β-hydroxy aliphatic azides. *Adv. Synth. Catal.* **365**, 342–354 (2023).
70. Xia, C.-X. et al. Photochemical Mn-mediated generation of azide radicals for improvement of alkene hydroxyazidation. *Org. Lett.* **26**, 3530–3535 (2024).


## Acknowledgements

This project was supported by the National Natural Science Foundation of China, Grant Nos. 22101265 (L.N.), 21903071 (S.-J.L.), 21822303 (Y.L.), and 22571284 (L.N.); China Postdoctoral Science Foundation Grant No. 2022M712866 (L.N.); Joint Fund of Key Technologies Research & Development Program of Henan Province, Grant Nos. 222301420006 (Y.L.) and 242301420053 (L.N.); Promotion Projects for Key Research & Development in Henan Province Grant No. 222102310042 (L.N.); The Ministry of Science and Technology of the People's Republic of China (Y.L.); Open Research Fund of State Key Laboratory of Coordination Chemistry, School of Chemistry and Chemical Engineering, Nanjing University (Y.L.); Open Cooperation Foundation of the Department of Chemical Science of Henan University (DCSHENU2401 S.L.). The authors are also grateful to the support from the Center of Advanced Analysis & Gene Sequencing of Zhengzhou University and Prof. Zhiguo Zhang.

## Author contributions

W.Y., Y.S., X.Y., Y.L., W.Z., S.-J.L., and L.N. conceived the work. W.Y., Y.S., X.Y., Y.-N.W., and L.N. designed the experiments and analyzed the data.

W.Y., Y.S., X.Y., M.T., X.J., and S.L. performed the synthetic experiments. W.Y., Y.S., and L.N. described manuscript and all authors revised.

## Competing interests
The authors declare no competing interests.

## Additional information
**Supplementary information** The online version contains supplementary material available at https://doi.org/10.1038/s41467-026-68837-y.

**Correspondence** and requests for materials should be addressed to Yu Lan, Wenjing Zhang, Shi-Jun Li or Linbin Niu.

**Peer review information** *Nature Communications* thanks the anonymous reviewers for their contribution to the peer review of this work. A peer review file is available.